Check for updates



ADVANCED FUNCTIONAL MATERIALS
www.afm-journal.de

# Composition-Reinforced Polydopamine Nanoenzyme for Improved Impairment of Prostatitis-Damaged Sexual Behavior and Enhanced Anti-Prostate Cancer

*Keyi Wang, Weipu Mao, Xinran Song, Wei Feng,* Guangchun Wang, Tao Zhang, Tianyuan Xu, Ming Chen, Yu Chen,* and Bo Peng**

**Inflammation is pivotal in the pathogenesis and progression of the most challenging diseases and even cancer. Nanomedicine-based strategy can be referred as a distinct solution to this complicated clinical obstacle by proposing an elaborated combination of effective therapeutic performances on inflammation and cancer. Herein, 2,2,6,6-tetramethylpiperidine-1-oxyl doped polydopamine nanoparticles, termed as TPDA NPs, with the significantly improved reactive oxygen/nitrogen species (RO/NSs) scavenging performance and enhanced photothermal efficiency are designed and synthesized by constructing donor-acceptor pairs, for prostate diseases treatment including anti-inflammation and anti-tumor. Benefiting from mimicking multi-natural enzymes, including superoxide dismutase, catalase, peroxidase, and glutathione peroxidase, TPDA NPs can inhibit the NF-$\kappa$B signaling pathways by downregulating the CD36 expression for the treatment of oxidative stress-induced prostatitis. Especially, TPDA NPs can improve the prostatitis-associated impairment of sexual behavior. By virtue of the enhanced photothermal-conversion efficiency, TPDA NPs ablate prostate cancer and simultaneously decrease inflammatory reaction. Therefore, this work provides a "three birds with one shot" paradigm to utilize rationally designed TPDA NPs for efficient management of prostate diseases.**

## 1. Introduction

Prostatitis is one of the most common diseases worldwide, which causes male health problems and adversely affects fertility.[1] Chronic prostatitis as the third type of prostatitis, is the most common classification accounting for more than 90% of patients with prostatitis, with a prevalence of 8.2% globally.[2] Activation of inflammatory reactions happened to the prostate induces the elevated expression of various inflammatory factors, such as interleukin-1 beta (IL-1$\beta$) and tumor necrosis factor-alpha (TNF-$\alpha$), resulting in the outbreak of reactive oxygen/nitrogen species (RO/NSs), which is an important pathogenic mechanism related to the clinical symptoms.[3] Notably, long-term exposure to excessive oxidative stress and RO/NSs overgeneration increases mutagenesis probability and facilitates epigenetic alteration in the prostate, leading to prostatic intraepithelial neoplasia and prostate cancer (PCa).[4] Moreover, inflammation plays a central role in some challenging diseases, especially cancer. Prostate cancer is the second most common cancer among men worldwide, with an incidence rate of 6.3 to 83.4 per 1 million men in various regions.[5] Since the early 1990s, the incidence of PCa has spiked to all-time highs and has plateaued recently. As the third-leading cause of death in men threatening long-term health and social homeostasis,[6] various treatment strategies for improving the survival rate

K. Wang, G. Wang, T. Xu, B. Peng
Department of Urology
Shanghai Tenth People's Hospital
School of Medicine
Tongji University
Shanghai 200072, P. R. China
E-mail: pengbo6908@tongji.edu.cn

W. Mao, M. Chen
Department of Urology
Affiliated Zhongda Hospital of Southeast University
Nanjing 210009, P. R. China

X. Song, W. Feng, Y. Chen
Materdicine Lab
School of Life Sciences
Shanghai University
Shanghai 200444, P. R. China
E-mail: fengw@shu.edu.cn; chenyuedu@shu.edu.cn

W. Feng, Y. Chen
Oujiang Laboratory (Zhejiang Lab for Regenerative Medicine Vision and Brain Health)
Wenzhou Institute of Shanghai University
Wenzhou, Zhejiang 325088, P. R. China

T. Zhang
Department of Urology
Putuo People's Hospital
School of Medicine
Tongji University
Shanghai 200060, China

The ORCID identification number(s) for the author(s) of this article can be found under https://doi.org/10.1002/adfm.202313528

DOI: 10.1002/adfm.202313528

 © 2024 Wiley-VCH GmbH

of PCa are highly desirable. Especially, to ensure therapeutic effectiveness and avoid various potential risks, simultaneous treatment of prostatitis and PCa is really challenging. However, the current therapies of anti-inflammation and anti-tumor would induce adverse side effects in the clinic. Immune modulators may also result in unpredictable systemic immune responses. Therefore, innovative and safe alternatives are required for the simultaneous treatment of prostatitis and PCa to ensure therapeutic effectiveness and avoid various potential risks.

The components of RO/NSs, such as hydroxyl (•OH), superoxide ($O_2^{\bullet -}$), hydrogen peroxide ($H_2O_2$), nitric oxide (NO•), and peroxynitrite ($ONOO^-$), could disrupt the balance of redox reaction and promote the outbreak of inflammatory factors, incorporating in the progression of various diseases, including inflammation, cancer, and neurodegenerative diseases.[7] Oxidative stress in prostate gland tissue could lead to the outbreak of RO/NSs, which are directly involved in the pathological process of prostatitis and PCa. It is confirmed that prostatitis promotes cancer formation by inflammation-related epigenetic alterations through RO/NSs.[4,8] Meanwhile, studies have shown that RO/NSs also play an essential role in male reproductive health.[9] All these studies have established that RO/NSs, as essential promoters, participate in the development and progression of prostate diseases. With the continuous development of nanotechnology, RO/NSs-based nanomedicine has made significant progress. Various nanomaterials with intrinsic enzyme-like characteristics, defined as nanozymes, have been synthesized to eliminate RO/NSs and treat multiple diseases,[7c,10] which exhibits the advantages of high catalytic activity, high stability, low cost, and easy to mass produce. Especially, the emergence of nanozyme has provided novel ideas for the treatment of various diseases by eliminating RO/NSs.[11] These nanomaterials can mimic first-line defense antioxidizes involving superoxide dismutase (SOD), catalase (CAT), and glutathione peroxidase (GPx) to efficiently reduce RO/NSs and restore the redox balance with the long-lasting and stable catalytic activity. Therefore, we envisage that the effective elimination of RO/NSs through multifunctional nanomaterials could alleviate the symptoms associated with inflammation and inhibit prostatitis, further protecting male fertility and preventing tumor generation.

Clinically, engineered 2,2,6,6-tetramethylpiperidine-1-oxyl (TEMPO) derivative has been applied in the prevention of radiation-induced toxicities and treatments of cardiovascular disease based on its SOD-like ability.[12] Inspiringly, herein, we propose reinforced polydopamine nanoparticles, termed as TPDA NPs, with the incorporation of TEMPO via a green one-step strategy to perform the anti-inflammation and anti-tumor function in prostate diseases. The introduction of TEMPO assisted in the construction of donor-acceptor pairs to improve the RO/NSs-scavenging ability and enhance the photothermal efficiency of traditional polydopamine NPs. They functioned as the multienzyme mimetics to effectively eliminate excess RO/NSs and further served as a robust photothermal agent to ablate cancer cells in tumor progression. RO/NSs overexpression was significantly scavenged through the multienzymes mimicking ability of TPDA, including SOD, peroxidase (POD), CAT, and GPx, further contributing to the protection of mitochondrial function and inhibition of inflammatory factors in mediating prostatitis through inhibiting the NF-$\kappa$B signaling pathways based on the downregulation of the CD36 expression. The inflammation-regulating activity of TPDA NPs further contributed to the recovery of fertility and sexual activities in experimental autoimmune prostatitis (EAP) rats. Additionally, TPDA NPs mediated antiinflammation and photothermal therapy (PTT) suppressed the tumor growth in vivo and assisted in restraining potential carcinogenesis in the prostate after long-term inflammation. Therefore, the rationally developed TPDA NPs not only feature the robust RO/NSs-scavenging capability, improved photothermal efficiency, and excellent biocompatibility, but also function as anti-inflammatory and anti-tumor agents with a prominent therapeutic effect for the treatment of prostate diseases (**Figure 1**).

## 2. Results and Discussion

### 2.1. Characterization of TPDA NPs

Traditional PDA NPs were prepared by the oxidative self-polymerization of dopamine (**Figure 2a**). Designed TPDA NPs were fabricated by using a facile and green one-pot TEMPO-mediated radical polymerization of dopamine (Figure 2a). Transmission electron microscopy (TEM) images demonstrated the well-dispersed spherical shape of TPDA and PDA NPs (Figure 2b; Figure S1, Supporting Information). The average hydrodynamic diameters of TPDA and PDA NPs are nearly the same around 200 nm, which is measured by dynamic light scattering (DLS) (Figure S2, Supporting Information). There are no obviously changes to the size at different time points, confirming the stability and dispersibility of TPDA NPs (Figure S3, Supporting Information). Energy dispersive X-ray spectrometry (EDS) elemental mapping images show the uniform distribution of C, N, and O elements in the TPDA NPs (Figure 2c). In the X-ray photoelectron spectroscopy (XPS) analysis, the peaks of C 1*s*, O 1*s*, and N 1*s* are observed in the survey spectra of TPDA and PDA NPs (Figure 2d; Figure S4, Supporting Information). The typical high-resolution XPS spectra of C 1*s* mainly contain three kinds of carbon bonds, including $sp^3$—C (C—C) at 285 eV, C═O at 288 eV, and C—O/C—N at 286 eV (Figure 2e; Figure S4, Supporting Information). Meanwhile, in the N 1*s* spectra, the peaks at 400 and 399 eV are assigned to C—N—C (pyrrolic nitrogen) and N—O, respectively (Figure 2f), with the detailed N—O peak that was not exhibited in the PDA NPs (Figure S5, Supporting Information), revealing the presence of TEMPO and pyrrolic ring. Moreover, the peaks in the O 1*s* region at 532 and 533 eV are corresponding to C═O and C—O/N—O (Figure 2g; Figure S5, Supporting Information), respectively. Compared with PDA NPs, a new characteristic peak at 1380 $cm^{-1}$ in the Fourier transform infrared (FTIR) spectra of TPDA NPs is indexed to the N—O stretching vibrations of TEMPO (Figure S6, Supporting Information). Meanwhile, the Raman spectra of PDA and TPDA NPs show that the broad bands at 1350 and 1580 $cm^{-1}$ are attributed to the stretching vibrations of hexagonal carbon rings in dopamine (Figure S7, Supporting Information). Like PDA NPs, the Zeta potential value of TPDA NPs is −30.1 mV, suggesting excellent stability and dispersity in solution due to the electrostatic repulsion (Figure S8).

Additionally, the blackness of TPDA NPs dispersion is much more obvious than that of PDA NPs dispersion at the same concentration, indicating that TPDA NPs possess stronger light


© 2024 Wiley-VCH GmbH

16163028, 0, Downloaded from https://onlinelibrary.wiley.com/doi/10.1002/adfm.202313528 by Tongji University, Wiley Online Library on [18/01/2024]. See the Terms and Conditions (https://onlinelibrary.wiley.com/terms-and-conditions) on Wiley Online Library for rules of use; OA articles are governed by the applicable Creative Commons License

16163028, 0, Downloaded from https://onlinelibrary.wiley.com/doi/10.1002/adfm.202313528 by Tongji University, Wiley Online Library on [18/01/2024]. See the Terms and Conditions (https://onlinelibrary.wiley.com/terms-and-conditions) on Wiley Online Library for rules of use; OA articles are governed by the applicable Creative Commons License

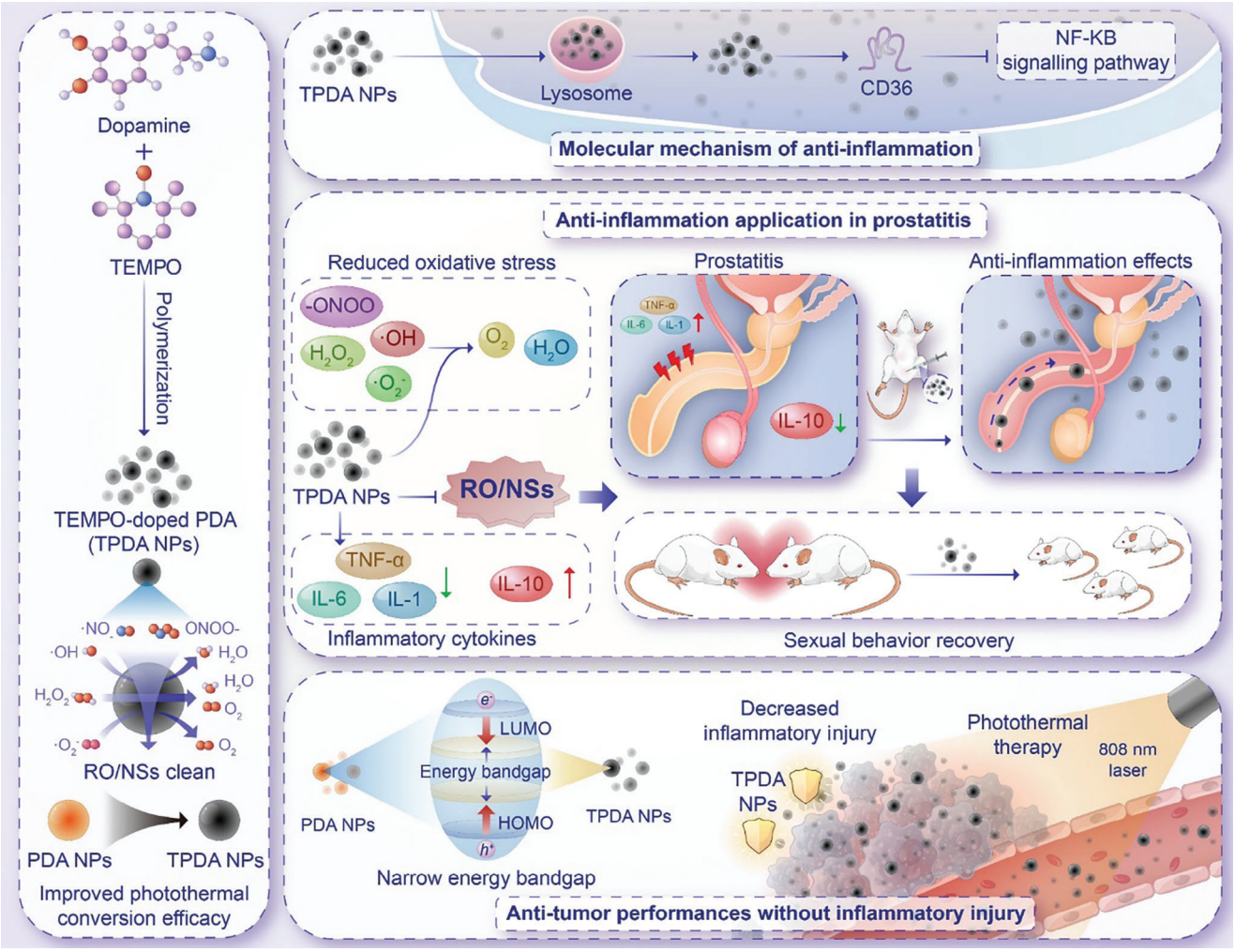


**Figure 1.** Schematic illustration of TPDA NPs against prostate diseases involving prostatitis, sexual injury, and prostate cancer, where TPDA NPs are prepared through a green one-step strategy, exhibiting narrower bandgap, boosted anti-oxidative ability, improved light absorption capacity, and enhanced photothermal conversion efficacy compared to traditional PDA NPs.

absorption performance than traditional PDA NPs (Figure S9, Supporting Information), which is further validated in the ultraviolet-near-infrared (UV-vis-NIR) absorbance spectra (Figure 2h). Importantly, the strong optical absorption capacity represents robust photothermal-conversion performance for nanomedicine. Meanwhile, the UV-vis-NIR absorption of TPDA dispersion varies little at different time points, further confirming the stability of TPDA NPs (Figure S10, Supporting Information). It is supposed that two pathways might follow the formation of TPDA NPs. In the first pathway, dopamine is oxidized by TEMPO to form dopamine-quinone, which leads to the intermediate generation of 5,6-indolequinone following the stages of intramolecular cyclization, oxidation to leucodopaminechrome and isomerisation to 5,6-dihydroxyindole[13] (Figure 2i). In the second pathway, TEMPO molecule is attached to the benzene ring of dopamine to form dopamine-TEMPO and then rearranged into 5,6-dihydroxyindole-TEMPO, which subsequently converts into the intermediates including (5,6-dihydroxyindole)2-TEMPO and/or (indole-5,6-quinone)2-TEMPO. Finally, all the intermediates involving 5,6-dihydroxyindole, (5,6-dihydroxyindole)2-TEMPO, and/or (indole-5,6-quinone)2-TEMPO are copolymerization to form the cross-linked macromolecular structure for TPDA NPs.

### 2.2. RO/NSs-Scavenging Activities of TPDA NPs

Next, we compared the total antioxidant capacity (TAC) between PDA and TPDA NPs using the typical 2,2′-azino-di (3-ethylbenzthiazoline-6-sulfonic acid) (ABTS) assay, which is expressed as Trolox equivalents. TAC is an analyte widely applied in the assessment of the antioxidant status existing in biological samples, which could measure the antioxidant ability towards free radicals.[14] An obvious concentration-dependent TAC value increase is observed in both PDA and TPDA NPs. Notably, compared with PDA NPs, TPDA NPs are gifted with much stronger ROS scavenging ability at the same concentration, suggesting that TEMPO-mediated polymerization can

 © 2024 Wiley-VCH GmbH

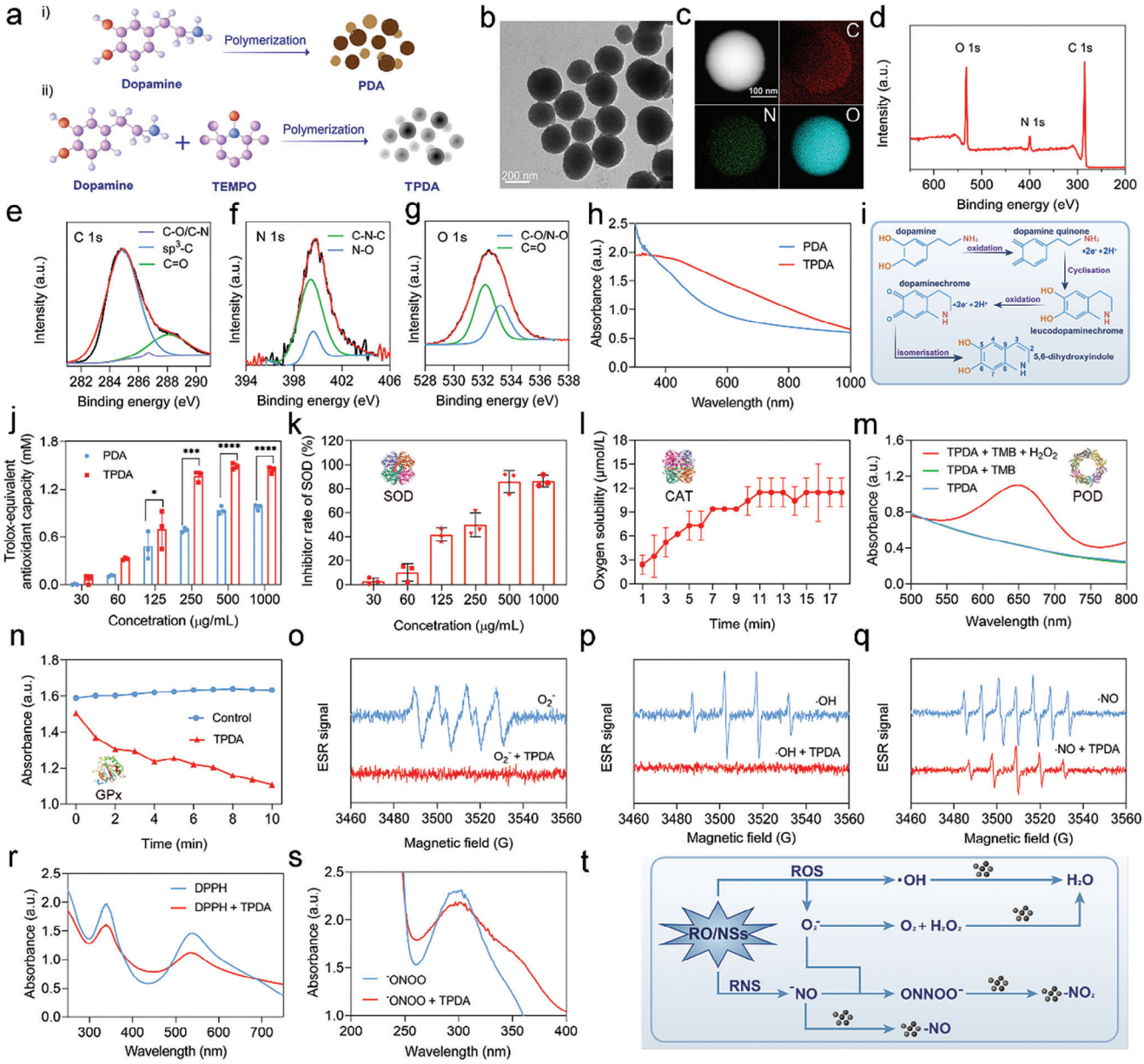


**Figure 2.** Characterization and RO/NS elimination performance of TPDA NPs. a) Schematic illustration of TPDA and PDA NPs preparation. b) TEM image of TPDA NPs. c) Scanning transmission electron microscopy (STEM) images with EDS mapping of C, N, and O elemental signals of TPDA NPs. d) XPS survey spectrum of TPDA NPs. High-resolution XPS spectra of e) C 1s, f) N 1s, and g) O 1s of TPDA NPs. h) UV-vis-NIR absorption spectra of PDA and TPDA NPs dispersion. i) Steps of TPDA NPs formation by dopamine oxidation. j) Total antioxidative capacity of PDA and TPDA NPs ($n = 3$ for each group). k) SOD-like activity of TPDA NPs ($n = 3$ for each group). l) CAT-like ability of TPDA NPs ($n = 3$ for each group). m POD-like activity of TPDA NPs ($n = 3$ for each group). n) GPx-like ability of TPDA NPs ($n = 3$ for each group). o) ESR spectra demonstrating $O_2^{\bullet-}$ elimination for TPDA NPs. p) ESR spectra demonstrating ●OH elimination for TPDA NPs. q) ESR spectra demonstrating $ONOO^-$ elimination for TPDA NPs. r RNS scavenging ability of TPDA NPs using DPPH● assay. s) $ONOO^-$ scavenging ability of TPDA NPs. t) Schematic illustration of RO/NSs-scavenging activities of TPDA NPs. Data presented as mean ± SD, and asterisks indicated significant differences (*$p < 0.05$, ***$p < 0.001$, and ****$p < 0.0001$) as compared with the control group using one-way analysis of variance (ANOVA).

improve the antioxidative level of PDA NPs, which contributes to the inflammation-mediating performances (Figure 2j). Subsequently, a series of representative antioxidant enzyme-mimetic activities of TPDA NPs were investigated. Superoxide dismutase (SOD) can promote the decomposition of $O_2^{\bullet-}$ to $H_2O_2$, which is essential in maintaining intracellular redox homeostasis. Since scavenging $O_2^{\bullet-}$ is the initial step of the anti-ROS cascade reaction, we initially focused on the SOD-like activity of TPDA NPs utilizing 2-(2-methoxy-4-nitrophenyl)−3-(4-nitrophenyl)−5-(2,4-disulfophenyl)−2H-tetrazolium sodium salt (WST-8) as an indicator. The results show that the percentage of produced formazan is decreased obviously in the presence of TPDA NPs,


© 2024 Wiley-VCH GmbH

16163028, 0, Downloaded from https://onlinelibrary.wiley.com/doi/10.1002/adfm.202313528 by Tongji University, Wiley Online Library on [18/01/2024]. See the Terms and Conditions (https://onlinelibrary.wiley.com/terms-and-conditions) on Wiley Online Library for rules of use; OA articles are governed by the applicable Creative Commons License

which is in a concentration-dependent manner, uncovering the SOD-like activity of TPDA NPs (Figure 2k).

Afterward, because $H_2O_2$ is important among biologically relevant ROS,[15] the catalase (CAT)-like activity of TPDA NPs is explored by converting $H_2O_2$ to $H_2O/O_2$ and detecting $O_2$ generation. The result demonstrates the enhancement of $O_2$ content with the extension of time after the addition of TPDA NPs (Figure 2l). Besides, the peroxidases (POD)-like activity of TPDA NPs is confirmed by choosing 3,5,3′,5′-tetramethylbenzidine (TMB) as the chromogenic substrate (Figure 2m). It is noteworthy that TPDA only exhibits POD activity in acidic conditions, nearly inactive in neutral and alkaline environments (Figure S11, Supporting Information), which is consistent with the previously reported nanozyme with POD-like activity.[16] Additionally, TPDA NPs are also featured with glutathione peroxidase (GPx) mimetic activity by oxidizing the reduced glutathione and scavenging $H_2O_2$ (Figure 2n). Taken together, TPDA NPs can mimic the activity of oxidoreductases such as SOD, CAT, POD, and GPx (Figure S12a, Supporting Information). Moreover, electron spin resonance (ESR) detection was carried out to further identify that TPDA NPs could effectively scavenge RO/NSs, including $O_2^{\bullet-}$, •OH, and $ONOO^-$ (Figure 2o–q). Apart from ROS, reactive nitrogen species (RNS) overgeneration can result in oxidative damage. Consequently, the RNS-eliminating capability of TPDA NPs was verified by employing 1,1-diphenyl-2-picrylhydrazyl radical (DPPH•) assay (Figure 2r; Figure S12b, Supporting Information). Furthermore, TPDA NPs exhibit benign $ONOO^-$ scavenging activity with evidence of absorption peak diminishment at 300 nm (Figure 2s; Figure S12c, Supporting Information). These anti-oxidative performances originate from the formation of quinone (3,5-di-tert-butyl-1,2-benzoquinone) which could react with radicals through the H-atom transfer mechanism.[17] It has been proved that the building block in PDA formation, indole-5,6-quinone-5,6-dihydroxyindole dimer, exhibited high reactivity toward hydroperoxyl radicals ($HOO^{\cdot}$), through trapping these radicals with the semiquinones and catechol groups. Meanwhile, TEMPO, functioning as the radical trapping agent, can promote the oxidative reaction through the plasmon coupling and electron transfer which further contributes to the anti-oxidative performances of TPDA NPs.[18] Therefore, the engineered biocompatible TPDA NPs feature prominent RO/NSs-scavenging ability response to various oxidative stress (Figure 2t).

### 2.3. Cytoprotection of TPDA NPs

Based on the satisfactory RO/NS-scavenging performance, TPDA NPs are expected to protect cells against oxidative damage (**Figure 3**a). The cytotoxicity of TPDA NPs was initially conducted by using Cell Counting Kit-8 (CCK-8) assay, which exhibits the excellent cytocompatibility of TPDA NPs even at the high concentration of 1000 μg $mL^{-1}$ (Figure S13, Supporting Information). Meanwhile, the red blood cell (RBC) hemolysis assay proves the benign hemocompatibility of TPDA NPs (Figure S14, Supporting Information). Besides, TPDA NPs can be internalized into the lysosomes by cells through endocytosis (Figure 3b and Movie S1) and function as protecting factors. This cellular uptake process is also confirmed by the bio-TEM which was conducted in the cells treated by the prepared TPDA NPs (Figure S15, Supporting Information). Lipopolysaccharide (LPS) can significantly inhibit RWPE-1 human prostate epithelial cell proliferation with a cell viability of 57% (Figure 3c). On the contrary, compared with the LPS group, TPDA NPs treatment can protect RWPE-1 cells from LPS-mediated oxidative damage, which is in a concentration-dependent manner. The cell viability is more than 80% following the treatment of TPDA NPs at 200 μg $mL^{-1}$ (Figure 3d). 5-ethynyl-2′-deoxyuridine (EdU) participating in the formation of newly synthesized DNA strands during cell replication is regarded as an indicator of proliferation. It is worth noting that the remarkable cell protective effect using TPDA NPs from LPS-induced cytotoxicity is validated by EdU, flow cytometry analysis, and live/dead co-staining (Figure 3e,f; Figure S16, Supporting Information), in which LPS-mediated cell death may result from intracellular RO/NS generation. After that, 2′,7′-dichlorofluorescein diacetate (DCFH-DA) and 4-amino-5-methylamino-2′,7′-difluorescein diacetate (DAF-FM DA) staining assays were conducted to measure intracellular RO/NS generation and identify the cytoprotective mechanism. Strong RO/NS-related fluorescent signals are detected in cells after LPS stimulation (Figure 3g). In contrast, weak intracellular fluorescence is observed in TPDA NPs-treated cells, demonstrating that TPDA NPs can significantly inhibit RO/NS overproduction.

Mitochondria, as the main aerobic respiratory unit, are susceptible to RO/NS imbalance, and excessive RO/NS could cause irrecoverable mitochondrial dysfunction thus triggering cell death. Subsequently, we assessed the mitochondrial superoxide generation and mitochondrial membrane potential (MMP) depolarization using MitoSOX mitochondrial superoxide indicator and 5′,6,6′-tetrachloro-1,1′,3,3′-tetraethylbenzimidazolylcarbocyanine iodide (JC-1) dye under confocal laser scanning microscopy (CLSM) examination. As expected, TPDA NPs can effectively alleviate LPS-caused mitochondria superoxide, and protect mitochondrial viability from MMP damage (Figure 3h). Given the significant anti-oxidative properties, we explored the cytokines expression in vitro to assess the anti-inflammation performance of TPDA NPs. In the presence of TPDA NPs, the expression of pro-inflammatory cytokines containing interleukin-1$\beta$ (IL-1$\beta$), interleukin-6 (IL-6), and tumor necrosis factor-$\alpha$ (TNF-$\alpha$), are distinctly diminished, revealing the anti-inflammatory effects of TPDA NPs (Figure 3i). Additionally, the expression of interleukin-10 (IL-10), an anti-inflammation cytokine, is elevated during the TPDA NPs treatment, which mitigates LPS-mediated inflammation (Figure 3i). All these results comprehensively uncover the distinguished cytoprotection capability of TPDA NPs through efficiently scavenging overexpressed RO/NSs, thereby diminishing inflammation and showing high potential in acute and chronic prostatitis therapy.

We further conducted RNA-sequencing to elucidate the molecular mechanisms underlying the TPDA NPs-based treatment (**Figure 4**a). There are 407 significantly differentially expressed genes (DEGs) between LPS group and LPS + TPDA NPs group, with 269 DEGs upregulated and 138 DEGs downregulated in the LPS + TPDA NPs group (Figure 4b; Figure S17, Supporting Information). Based on the total DEGs, we performed the Kyoto Encyclopedia of Genes and Genomes (KEGG) and Gene Ontology analysis (Figure 4c). TPDA NPs treatment could alter the gene enrichment in response to interferon, cytokine receptor binding,


© 2024 Wiley-VCH GmbH

16163028, 0, Downloaded from https://onlinelibrary.wiley.com/doi/10.1002/adfm.202313528 by Tongji University, Wiley Online Library on [18/01/2024]. See the Terms and Conditions (https://onlinelibrary.wiley.com/terms-and-conditions) on Wiley Online Library for rules of use; OA articles are governed by the applicable Creative Commons License

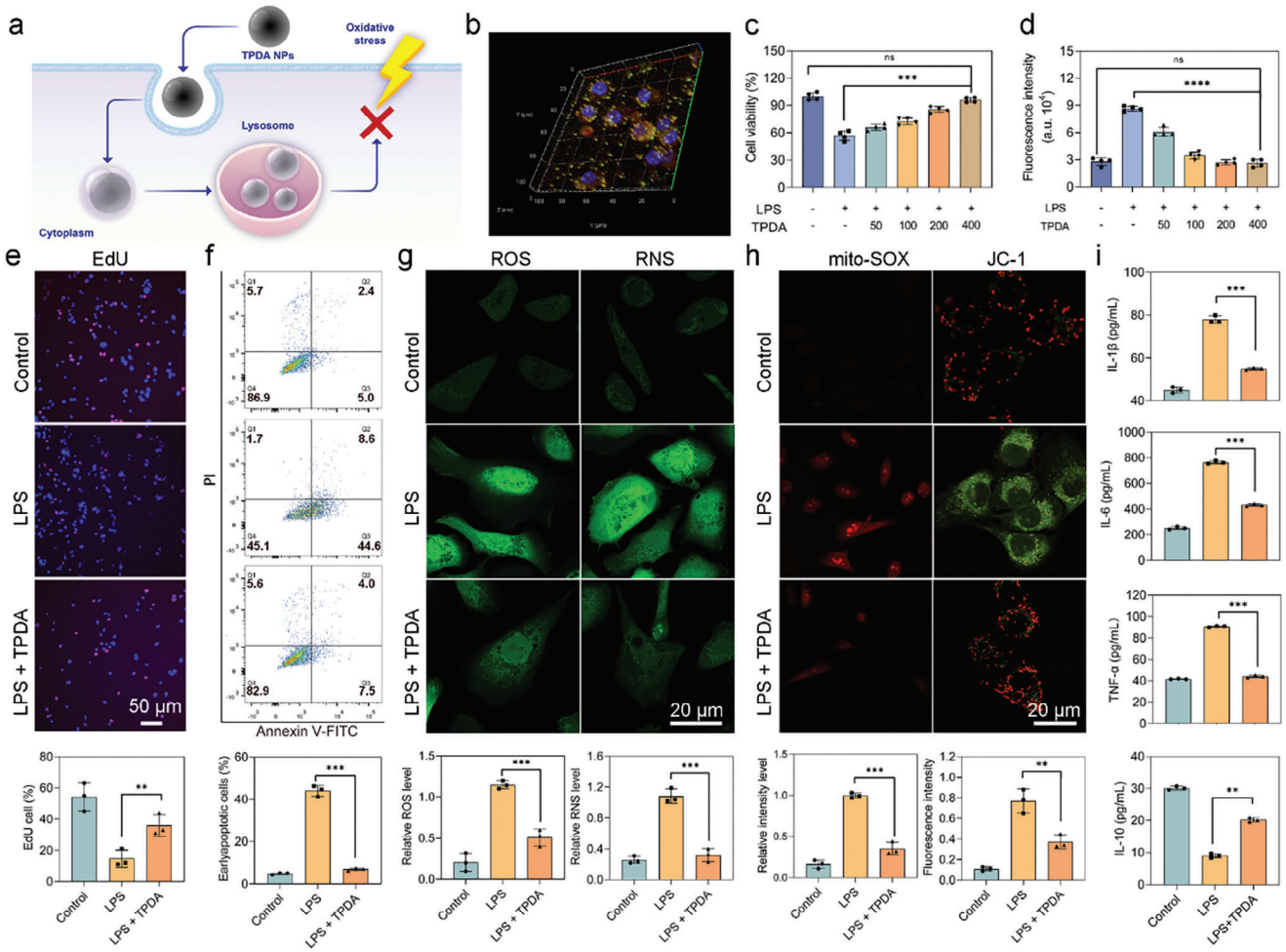


**Figure 3.** Anti-oxidation in vitro and cytoprotection of TPDA NPs. a) Schematic illustration of the cytoprotective performance of TPDA NPs. b) Cellular internalization of TPDA NPs through endocytosis. c) TPDA NPs protect RWPE-1 cells from LPS-induced oxidative stress ($n = 4$ for each group). d) TPDA NPs inhibit ROS overgeneration from LPS-induced cell damage ($n = 4$ for each group). e) CLSM images after EdU staining following different treatments. f) Flow cytometry analysis of cells after different treatments using apoptosis detection kit. g) CLSM images of RWPE-1 cells after different treatments stained with DCFH-DA and DAF-FM DA. h) CLSM images of RWPE-1 cells after different treatments stained by MitoSOX and JC-1. i) Inflammatory factors including IL-1$\beta$, IL-6, TNF-$\alpha$, and IL-10 expression changes in RWPE-1 cells after different treatments ($n = 3$ for each group). Data presented as mean ± SD, and asterisks indicated significant differences (**$p < 0.01$ and ***$p < 0.001$) as compared with the control group using one-way analysis of variance (ANOVA).

cytokine-cytokine receptor interaction, and membrane region, which confirms that the TPDA NPs significantly improve the cellular defenses towards LPS-induced oxidative stress. Subsequently, the detailed KEGG annotation is presented (Figure 4d), indicating that TPDA NPs can enhance the immune response to oxidative damage, which is also confirmed by the Gene Set Enrichment Analysis (GSEA) (Figure S18, Supporting Information). Meanwhile, Gene Ontology analysis exhibits that inflammatory responses to LPS-induced damages are augmented in the TPDA NPs treatment group (Figure 4e). The transcription factors (TFs) related to the DEGs were further analyzed to assess the cellular gene changes after the TPDA NPs treatment (Figure 4f). It is found that most DEGs are regulated by NF-$\kappa$B1, indicating its involvement in cellular protection upon the TPDA NPs treatment. The enriched chord diagram of DEGs involves regulating NF-$\kappa$B signaling, response to external stimulus, and immune system process, which is applied in the screening process to concentrate on the vital functional DEG in the TPDA NPs treatment (Figure 4g). It could be inferred that, among the analyzed DEGs, CD36 (cluster of differentiation 36) could regulate the nuclear factor (NF)-$\kappa$B signal pathway.[19] TPDA NPs not only effectively decrease the overexpression of CD36 mRNA (Figure S19, Supporting Information), but also inhibit the expression of CD36 protein and NF-$\kappa$B signal pathway-related proteins such as p65, p-p65, ikB, and p-ikB (Figure S20, Supporting Information), which is confirmed by mRNA expression and western blot analysis, demonstrating that TPDA NPs can target CD36 to regulate NF-$\kappa$B signaling pathway for anti-inflammation. CD36, a scavenger receptor, has been considered as the promotor of inflammatory stress through stimulating nuclear translocation and phosphorylation of p65, further activating the NF-$\kappa$B pathway.[19d] Meanwhile, IkB phosphorylation participates in NF-$\kappa$B pathway


© 2024 Wiley-VCH GmbH

16163028, 0, Downloaded from https://onlinelibrary.wiley.com/doi/10.1002/adfm.202313528 by Tongji University, Wiley Online Library on [18/01/2024]. See the Terms and Conditions (https://onlinelibrary.wiley.com/terms-and-conditions) on Wiley Online Library for rules of use; OA articles are governed by the applicable Creative Commons License

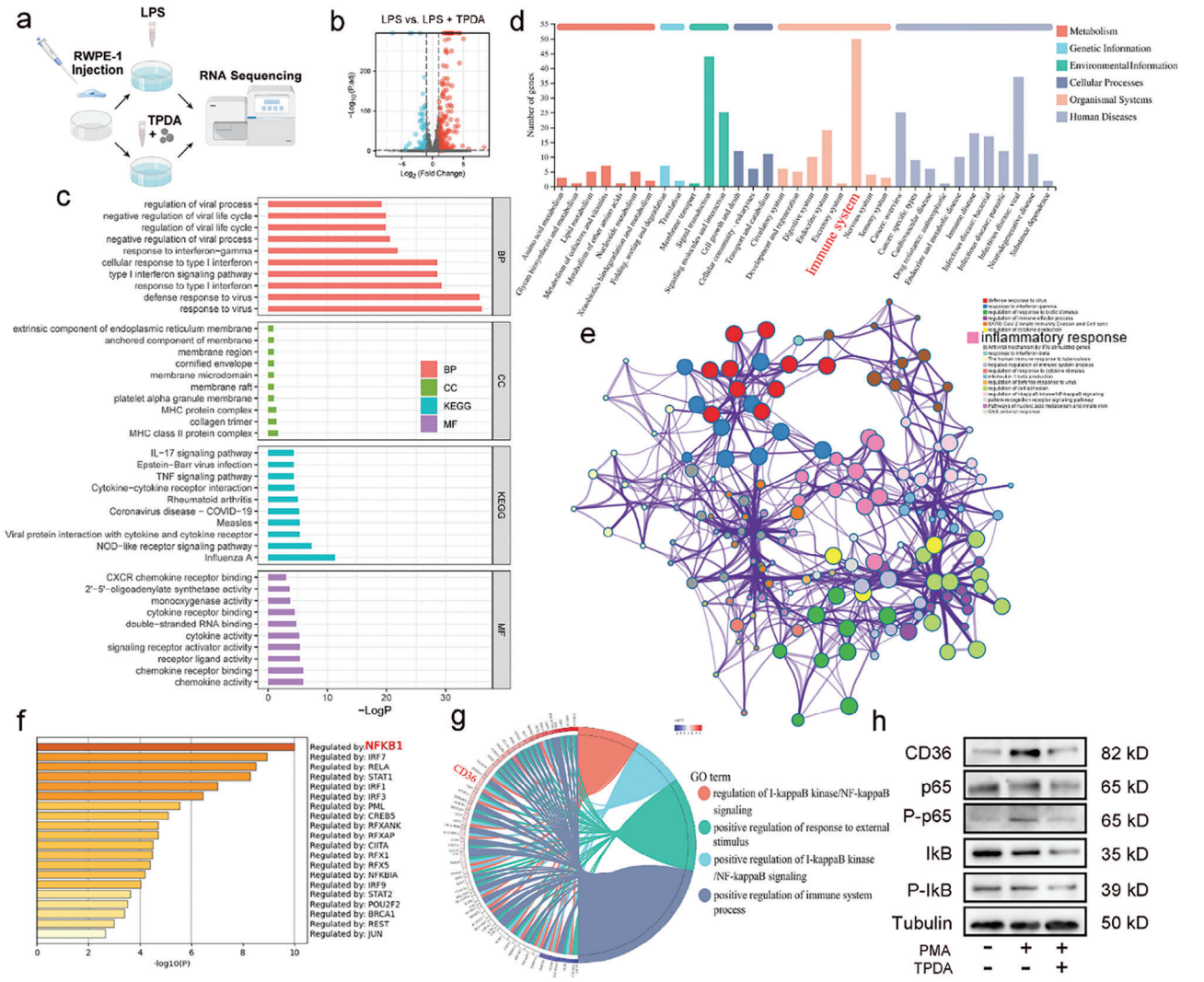


**Figure 4.** Anti-oxidative mechanisms of TPDA NPs-treated LPS-induced inflammation. a) Schematic illustration of RNA sequencing. b) Volcano plots exhibiting the up or down-regulation DEGs in this sequencing results. c) Gene Ontology and KEGG analysis of the DEGs in the LPS-treated RWPE-1 cells with or without TPDA NPs protection. d KEGG annotation of the total DEGs. e) Gene Ontology clusters based on the total DEGs in the LPS-treated RWPE-1 cells with or without TPDA NPs protection. f) Analyzation of the TFs in the DEGs regulation. g) Enriched chord diagram of the Gene Ontology analyses. h) Western blot analysis of CD36, p65, p-p65, ikB, and p-ikB in REPE-1 cells after different treatments.

activation in a variety of disease states through binding with NF-$\kappa$B 1 to form functional protein complexes. TPDA NPs function as the CD36 inhibitor that could regulate the NF-$\kappa$B signal pathway and eliminate inflammatory damage in response to oxidative stress. Furthermore, following an NF-$\kappa$B signaling pathway activator phorbol-12-myristate-13-acetate (PMA) stimulation, levels of CD36, p65, p-p65, ikB, and p-ikB are reduced in TPDA NPs-treated cells (Figure 4h; Figure S21, Supporting Information), further consolidating the finding that TPDA NPs regulate the NF-$\kappa$B signaling pathway by targeting CD36.

### 2.4. TPDA NPs Against Prostatitis In Vivo

Ahead of disease treatment, we next assessed the in vivo toxicity of TPDA NPs to confirm their biocompatibility. Hematoxylin & eosin (H&E) stained the main organs, including the heart, liver, spleen, lung, and kidney, which revealed no notable morphological defects in the TPDA NPs group, demonstrating excellent biocompatibility of TPDA NPs (Figure S22, Supporting Information). All the serum tests, including the number of red blood cells, white blood cells, and platelets, further prove that TPDA NPs injection i.v. leads to no obvious damage to the hematopoietic and immune systems in vivo (Figure S23–S25, Supporting Information).

LPS-induced acute prostatitis models were next established to assess the anti-inflammation activity of TPDA NPs in vivo (**Figure 5a**).[20] Eighteen ICR mice were randomly divided into three groups: control, LPS, and LPS + TPDA NPs group. During 7 days of observation, LPS-induced prostatitis mice display a decreased body weight. Notably, the body weight is improved after TPDA NPs treatment (Figure S26, Supporting Information). LPS


© 2024 Wiley-VCH GmbH

16163028, 0, Downloaded from https://onlinelibrary.wiley.com/doi/10.1002/adfm.202313528 by Tongji University, Wiley Online Library on [18/01/2024]. See the Terms and Conditions (https://onlinelibrary.wiley.com/terms-and-conditions) on Wiley Online Library for rules of use; OA articles are governed by the applicable Creative Commons License

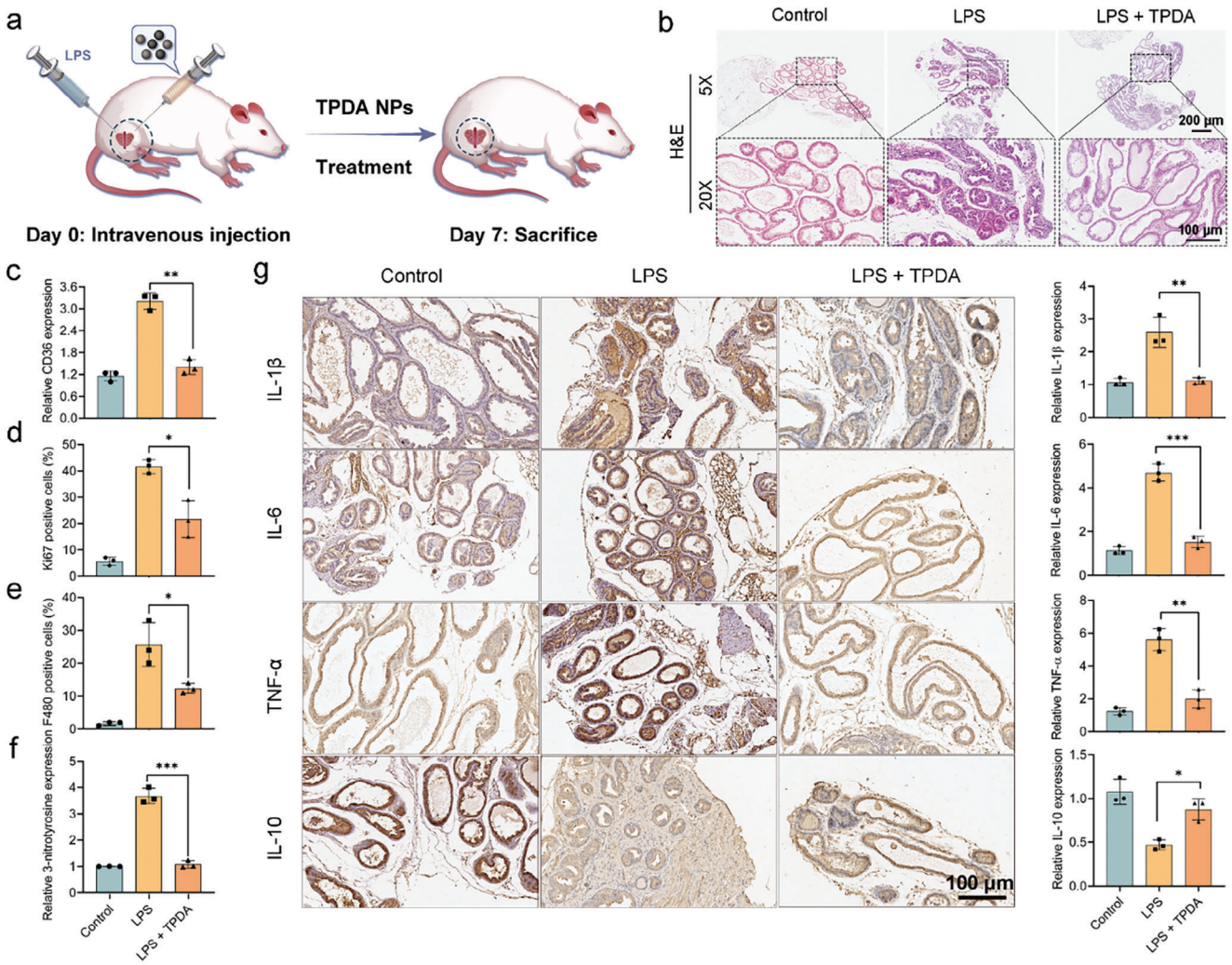


**Figure 5.** Acute prostatitis treatment based on TPDA NPs in vivo. a) Schematic illustration of acute prostatitis model establishment and treatment schedule. b) H&E staining images of the prostate after different treatments. c) Corresponding quantitative analysis of CD36 expression in different groups ($n = 3$ for each group). Relative expression analysis of d Ki67 positive cells, e) F480 positive cells, and f 3-nitrotyrosine in different groups ($n = 3$ for each group). g) Immunohistochemical staining images and relative expressions of IL-1$\beta$, IL-6, TNF-$\alpha$, and IL-10 in different groups ($n = 3$ for each group). Data presented as mean ± SD, and asterisks indicated significant differences ($^*p < 0.05$, $^{**}p < 0.01$ and $^{***}p < 0.001$) as compared with the control group using one-way analysis of variance (ANOVA).

results in prostatitis and significantly increases the alveolar hyperplasia and immune cell infiltration in the gland lumen based on the H&E staining results, whereas the symptoms can be effectively alleviated in the mice treated with TPDA NPs (Figure 5b). Furthermore, CD36 expression decreases to the normal level after TPDA NPs treatment (Figure 5c; Figure S27, Supporting Information). Moreover, prostatitis alleviation is demonstrated with an inhibited positive ratio of proliferating cells stained with Ki67 (Figure 5d; Figure S27, Supporting Information). Besides, the increased macrophages which were marked by F480, can be inhibited by TPDA NPs in vivo (Figure 5e; Figure S27, Supporting Information). Furthermore, nitrotyrosine staining, a biomarker of peroxynitrite-caused nitration, was employed to evaluate the level of oxidative damage. The nitrotyrosine expression is typically suppressed following TPDA NPs treatment (Figure 5f and Figure S27, Supporting Information). Consistently, the expressions of IL-1$\beta$, IL-6, TNF-$\alpha$, and IL-10 are significantly decreased, and the level of IL-10 is prominently augmented in the prostate of TPDA NPs-treated prostatitis mice (Figure 5g).

### 2.5. Effect of TPDA NPs on Male Rats' Sexual Behaviors

We further explored TPDA NPs treatment for chronic prostatitis in the experimental autoimmune prostatitis (EAP) rat model,[21] which was established through the subcutaneous administration of prostate tissue homogenate supernatant (PTHS) and Freund's complete adjuvant (FCA) (**Figure 6**a). Compared with the control group, EAP rats after TPDA NPs treatment exhibit decreased alveolar hyperplasia and declined proliferating cells in the gland of the prostrate (Figure 6b; Figure S28, Supporting Information). Meanwhile, the decreased IL-1$\beta$, IL-6, and TNF-$\alpha$, along


© 2024 Wiley-VCH GmbH

16163028, 0, Downloaded from https://onlinelibrary.wiley.com/doi/10.1002/adfm.202313528 by Tongji University, Wiley Online Library on [18/01/2024]. See the Terms and Conditions (https://onlinelibrary.wiley.com/terms-and-conditions) on Wiley Online Library for rules of use; OA articles are governed by the applicable Creative Commons License

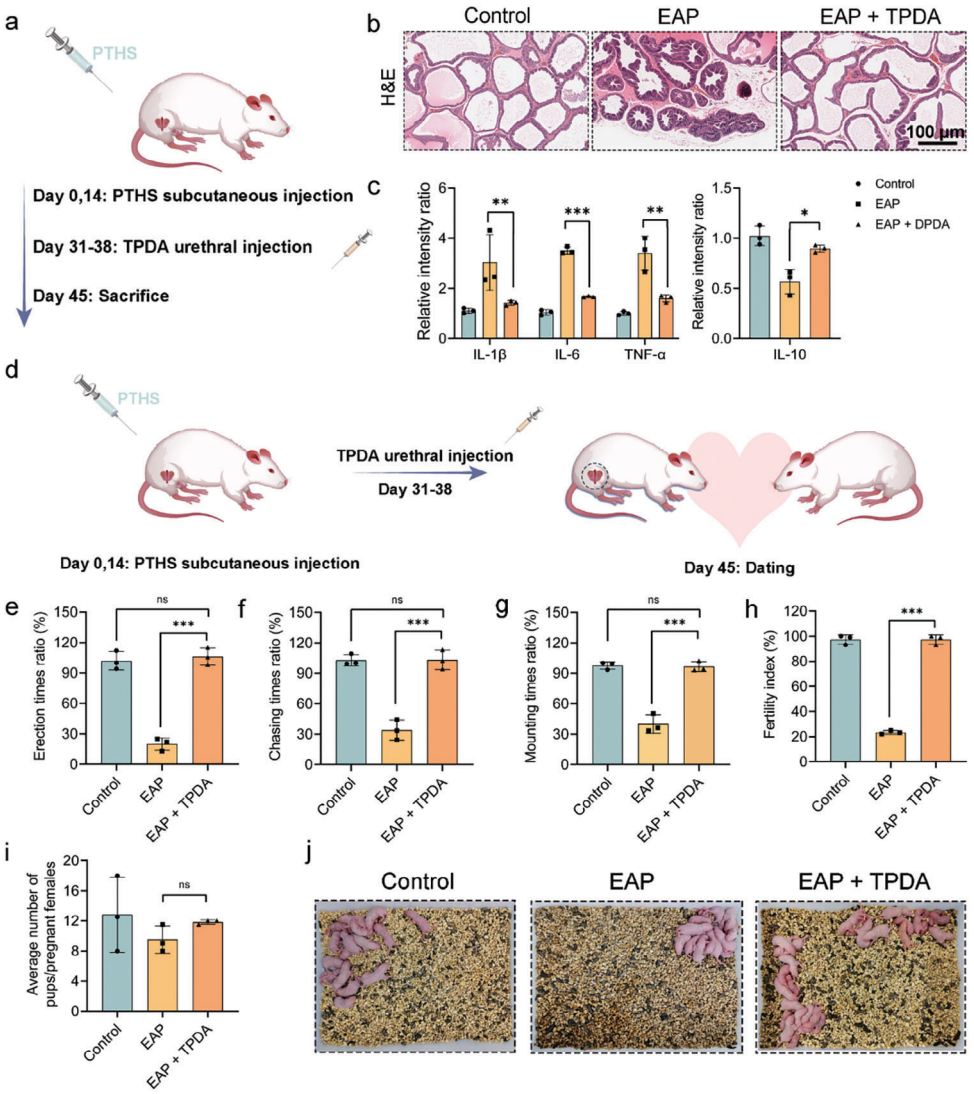


**Figure 6.** Inhibition of inflammatory injuries of EAP by TPDA NPs in vivo. a) Schematic illustration of anti-inflammation in EAP rats. b) H&E staining of the prostate after different treatments. c) Expression changes of IL-1$\beta$, IL-6, TNF-$\alpha$, and IL-10 in the penis after different treatments ($n = 3$ for each group). d) Schematic illustration of fertility assessment in EAP rats. Examination results of e) erection rate, f) chasing time ratio, and g) mounting time of the rats after different treatments ($n = 3$ for each group). h) Fertility index of male rats in the three subgroups ($n = 3$ for each group). i) Average number of pups/pregnant females after different treatments ($n = 3$ for each group). j) Corresponding offspring in the three subgroups. Data presented as mean ± SD, and asterisks indicated significant differences (***$p < 0.001$) as compared with the control group using one-way analysis of variance (ANOVA).

with the elevated IL-10 are detected following TPDA NPs treatments (Figure S29, Supporting Information), demonstrating the inflammation inhibition in the prostate of EAP rats. Additionally, we investigated the inflammation in the penis. Although H&E staining shows inapparent oxidative injury such as immune cell infiltration in the penile tissues (Figure S30, Supporting Information), the increased TdT-mediated dUTP Nick-End Labeling (TUNEL) stained positive cells reveal the inflammatory damage in penile tissues in EAP rats, which can be effectively reversed after TPDA NPs treatments (Figure S30, Supporting Information). The inflammatory cytokine levels of IL-1$\beta$, IL-6, TNF-$\alpha$, and IL-10 tend to be normal, confirming the protective effects of TPDA NPs (Figure 6c; Figure S31, Supporting Information).

Moreover, clinical and epidemiological results of CP/CPPS show that EAP induces erectile dysfunction (ED) and impacts fertility in rats.[21b,e,22] Next, a series of experiments were conducted to estimate the effects of TPDA NPs treatment on sexual behaviors (Figure 6d). It is exhibited that damaged sexual behaviors of erectile function and mating performances exist in EAP rats, which was improved following TPDA NPs treatment (Figure 6e–g). The erection rate increases from ≈30% to ≈95% after TPDA NPs treatments, indicating improved penile function after the inflammation mediation (Figure 6e). The chasing time ratio and mounting time ratio are effectively improved after TPDA NPs treatment, proving the higher sexual excitement of mating (Figure 6f,g). We next assessed the reproductive


© 2024 Wiley-VCH GmbH

16163028, 0, Downloaded from https://onlinelibrary.wiley.com/doi/10.1002/adfm.202313528 by Tongji University, Wiley Online Library on [18/01/2024]. See the Terms and Conditions (https://onlinelibrary.wiley.com/terms-and-conditions) on Wiley Online Library for rules of use; OA articles are governed by the applicable Creative Commons License

ability of these mice. It is noteworthy that the fertility index of EAP group decreased to ≈30% with nearly one-third EAP rats successfully obtaining their offspring, which is effectively improved after TPDA NPs treatment (Figure 6h). However, the number of pups from the pregnant female rat was almost the same in the three groups without observable defects in each pup (Figure 6i,j). Besides, the pups exhibit similar weight after two months of breeding, showing no morphological differences (Figure S32, Supporting Information). Besides, an H&E examination of the testis and epididymis was conducted to evaluate sperm production among the three subgroups. There is no degeneration or disorder of spermatogenic cells including spermatocytes and spermatozoa in the testis, and the mature sperms show no differences in the epididymis (Figure S33, Supporting Information). Furthermore, almost no difference in the morphology, survival rate, and sperm motility are observed after different treatments (Figure S34 and S35 and Movie S2–S4, Supporting Information). These performances comprehensively confirm the biocompatibility of TPDA NPs in vivo, which further promotes the clinical translation of TPDA NPs in the future treatment of inflammatory diseases. All these results indicate that TPDA NPs can improve ED by relieving penile inflammation, which could contribute to the advancement of clinical therapy.

### 2.6. Anti-Tumor Performances of Improved PTT Combined with Inflammation Regulation by TPDA NPs

Inflammation, especially chronic inflammation, is closely associated with tumorigenesis and progression.[23] Actually, prostatitis is one of the important causes of prostate carcinogenesis. Therefore, the antitumor agents possessing intrinsic anti-inflammation function could enhance the therapeutic efficiency and prognosis of prostate cancer in the clinic, which promoted us to evaluate the ability of TPDA NPs for anti-tumor therapy and tumor microenvironment modulation. As above-mentioned, the light absorption of TPDA NPs is significantly stronger than conventional PDA NPs, which contributes to the improved photothermal performance of tumor PTT.

As expected, at the concentration of 60 μg/mL, the temperature elevation of TPDA NPs is up to 62 °C, which is much higher than 54 °C of PDA NPs, confirming TEMPO addition can enhance the photothermal conversion ability of PDA NPs (**Figure** 7a). Furthermore, the photothermal effect of TPDA NPs is in a concentration and laser power density-dependent manner (Figure 7b,c), meanwhile possessing benign photothermal stability (Figure 7d,e). The photothermal conversion efficiency of TPDA NPs is calculated to be 29.2% (Figure S36a, Supporting Information), which is higher than traditional PDA NPs (13.1% ≈17.6%)[24] and Au nanorods (22%),[25] further indicating the improved photothermal performance of TPDA NPs. Meanwhile, the extinction coefficient ($\epsilon$) of TPDA NPs is calculated to be 18.1 L $g^{-1}$ $cm^{-1}$ according to the Lambert–Beer law (Figure S36b, Supporting Information). Additionally, the photothermal performance parameters of several classic photothermal agents have been summarized in Table S1 (Supporting Information), which shows the noticeable photothermal conversion efficiency of TPDA NPs compared to the reported photothermal agents.

To explicate the underlying mechanism of enhanced light absorption and light-to-heat ability of TPDA NPs, the detailed structural analysis was carried out by calculating the energy bandgap using the density functional theory (DFT) method. It is hypothesized that the microstructures of TPDA NPs are based on the typical chemical conjugates among four possible oligomers involving $C_1$, $C_2$, $C_3$, and $C_4$ based on the permutation and combination of TEMPO, 5,6-dihydroxyindole and indole-5,6-quinone (Figure 7f). The LUMO/HOMO energy levels (EHOMO/ELUMO) of $C_1$, $C_2$, $C_3$, and $C_4$ are calculated to be −1.06 eV/−3.73 eV, −3.95 eV/−4.72 eV, −1.02 eV/−3.48 eV, and −3.81 eV/−4.53 eV, respectively, and their bandgaps are calculated to be 2.67, 0.77, 2.64, and 0.72 eV, respectively. The improved electron delocalization and decreased bandgap following TEMPO addition lead to better electron delocalization and stronger light absorption capacity. With enhanced light absorbance, the TPDA NPs are expected for cancer PTT. Subsequently, in vitro TPDA NPs-mediated PTT was evaluated using PC-3 human prostate cancer cells. After PTT, the cell viability shows that increased concentration leads to more significant cell death and less than 20% cancer cell survival after treatment with TPDA NPs at 200 μg $mL^{-1}$ under laser irradiation (Figure 7g). Besides, the remarkable cancer cell-killing effect of TPDA NPs-induced PTT is verified by EdU staining, colony experiment, live/dead co-staining, and flow cytometry analysis (Figure 7h–j; Figure S37, Supporting Information).

Inspired by the robust anti-inflammation and photothermal performance, the anti-tumor in vivo was carried out on luciferin-labeled PC-3 tumor-bearing mice (**Figure** 8a). Polyethylene glycol (PEG) modified graphene oxide nanosheets (GO NSs) with photothermal conversion ability without anti-inflammation properties were employed as a positive control.[26] The PC-3 tumor-bearing mice were randomly divided into five groups: control group, laser group, TPDA NPs group, TPDA NPs + laser group, and GO NSs + laser group. The real-time temperature of the tumor region was monitored by using an infrared thermal imaging camera. Apparently, the tumor temperatures of TPDA NPs and GO NSs treated mice under 808 nm laser irradiation increase quickly and reach 55°C within 10 min, whereas that of the control groups exhibit less obvious temperature elevation (Figure 8b,c). The tumor volumes and body weights of mice among the different treatments were recorded every 2 days. No significant weight changes were measured in the tumor-bearing mice after different treatments, indicating the high therapeutic biosafety of TPDA NPs (Figure 8d). Meanwhile, the excellent biocompatibility of TPDA NPs also indicates the high potential in the clinical translation for tumor treatments.

After diverse treatments, compared with the control group, the TPDA NPs group and laser group display no visible therapeutic outcome (Figure 8e–h). In contrast, the TPDA NPs + laser group and GO NSs + laser group can markedly inhibit tumor growth (Figure 8j), with inhibition rates of 92.1% in the TPDA NPs + laser group and 91.8% in the GO NSs + laser group (Figure 8k). Besides, the in vivo imaging system (IVIS) results and photographs of the dissected tumor tissues from different treatment groups visualized the notable anti-tumor efficacy of PTT (Figure 8l). The underlying therapeutic mechanism was further investigated through H&E, Ki67, and TUNEL staining (Figure 8i; Figure S38, Supporting Information). Tumor cells


© 2024 Wiley-VCH GmbH

16163028, 0, Downloaded from https://onlinelibrary.wiley.com/doi/10.1002/adfm.202313528 by Tongji University, Wiley Online Library on [18/01/2024]. See the Terms and Conditions (https://onlinelibrary.wiley.com/terms-and-conditions) on Wiley Online Library for rules of use; OA articles are governed by the applicable Creative Commons License

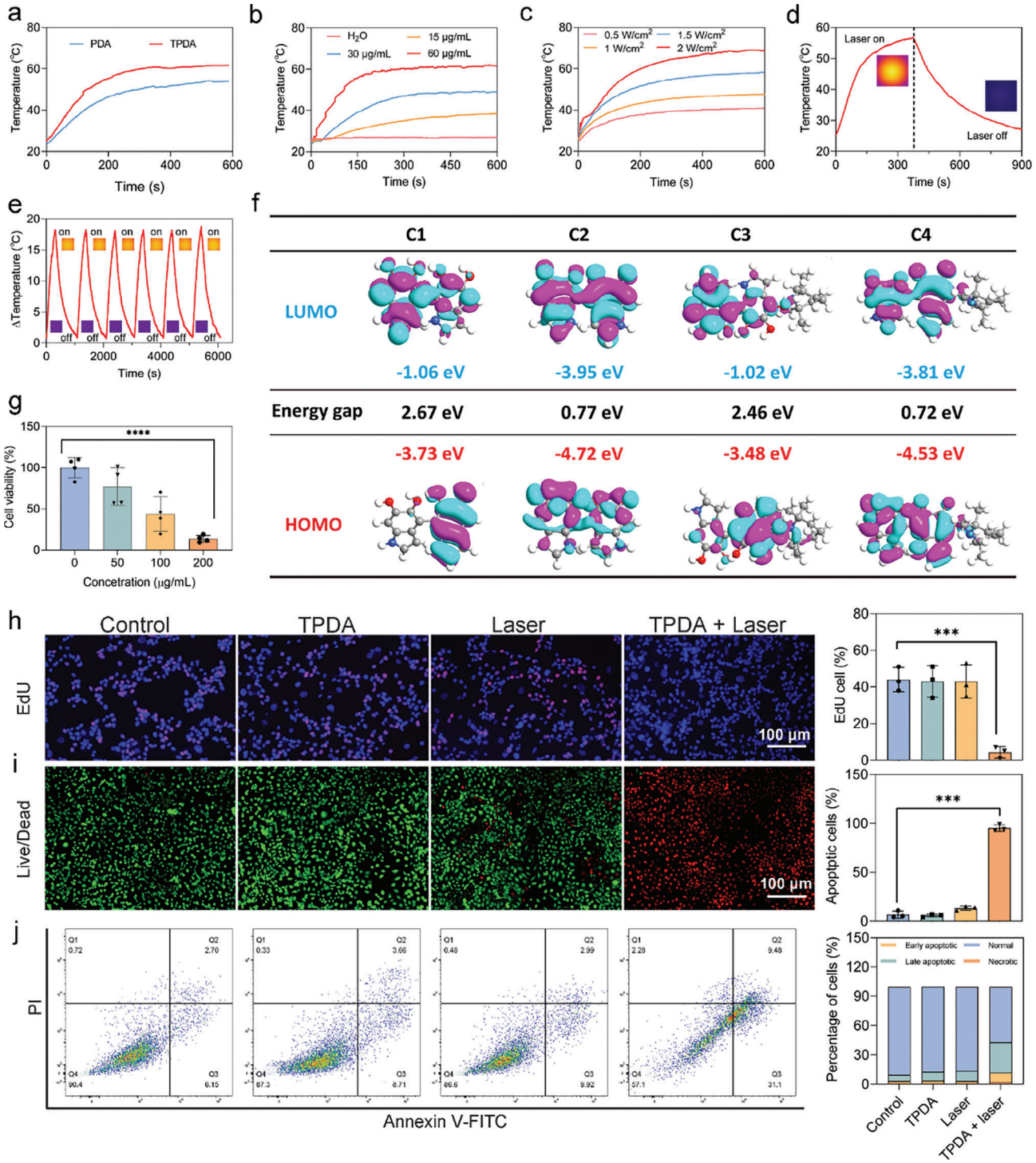


**Figure 7.** Photothermal performance and TPDA NPs-mediated PTT in vitro. a) Photothermal conversion performance of PDA and TPDA NPs at the concentration of 60 μg $mL^{-1}$ under 808 nm laser irradiation. b) Photothermal heating curves of TPDA NPs dispersion with different concentrations under 808 nm laser irradiation. c) Photothermal heating curves of TPDA NPs at 60 μg $mL^{-1}$ under 808 nm laser irradiation with different power densities. d) Heating and cooling curves of TPDA NPs dispersion under 808 nm laser irradiation on and off. e) Heating and cooling curve of TPDA NPs dispersion under 808 nm laser irradiation for six cycles. f DFT measurement of TPDA, indicating that TPDA contains a lower energy bandage than conventional PDA. g) Cell viabilities of PC-3 cells after treatment with TPDA NPs with different concentrations under 808 nm laser irradiation ($n = 4$ for each group). h) EdU staining results and corresponding quantitative analysis of PC-3 cells after different treatments ($n = 3$ for each group). i) Live/dead staining and the corresponding quantitative analysis of PC-3 cells after different treatments ($n = 3$ for each group). j) Flow cytometry analysis of cell apoptosis after different treatments. Data presented as mean ± SD, and asterisks indicated significant differences (***$p < 0.001$ and ****$p < 0.0001$) as compared with the control group using one-way analysis of variance (ANOVA).



© 2024 Wiley-VCH GmbH

16163028, 0, Downloaded from https://onlinelibrary.wiley.com/doi/10.1002/adfm.202313528 by Tongji University, Wiley Online Library on [18/01/2024]. See the Terms and Conditions (https://onlinelibrary.wiley.com/terms-and-conditions) on Wiley Online Library for rules of use; OA articles are governed by the applicable Creative Commons License

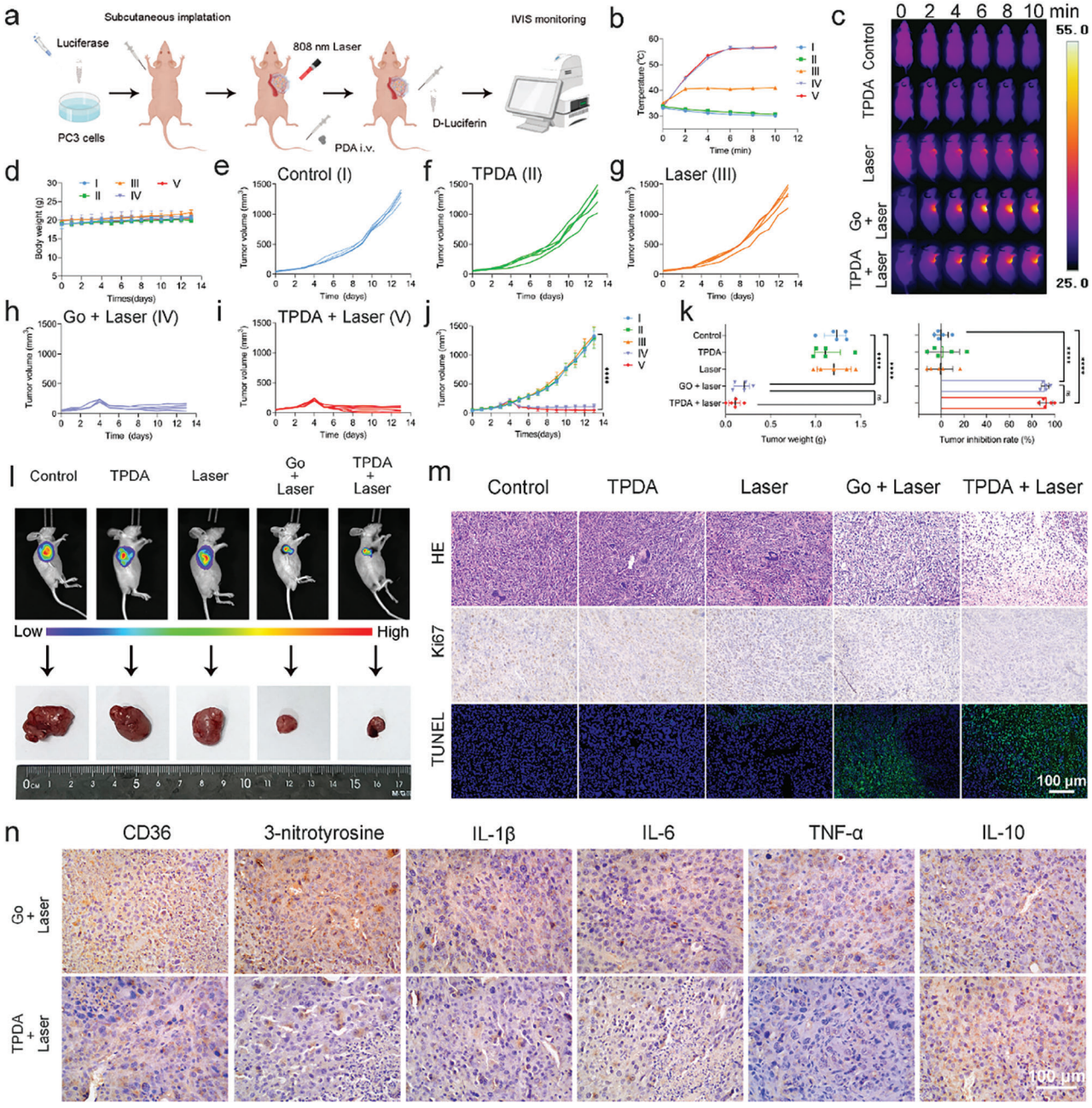


**Figure 8.** Anti-tumor effect of TPDA NPs in vivo. a) Schematic illustration of anti-tumor performances in PC-3 tumor-bearing mice. b) Tumor temperature elevation curves, and c) thermal images of tumors after the different treatments at designed time points. d) Body weight changes of the mice recorded during the treatments ($n = 5$ for each group). Individual tumor growth curves in the different subgroups including e) control, f) TPDA NPs, g) 808 nm laser irradiation, h) GO NSs under 808 nm laser irradiation, and i) TPDA NPs under 808 nm laser irradiation. j Tumor volumes, k) Tumor weights and tumor inhibition rates in PC-3 tumor-bearing mice after different subgroups ($n = 5$ for each group). l) IVIS images and the dissected tumor photos of the tumor dissected from PC-3 tumor-bearing mice after different treatments. m H&E, Ki-67, and TUNEL staining results of the tumors from different groups. n) The IHC results of CD36, 3-nitrotyrosine, IL-1$\beta$, IL-6, TNF-$\alpha$, and IL-10 expression in the tumors from the two groups of GO NSs under 808 nm laser irradiation and TPDA NPs under 808 nm laser irradiation. Data presented as mean ± SD, and asterisks indicated significant differences (****$p <$ 0.0001) as compared with the control group using one-way analysis of variance (ANOVA).

are severe necrosis with deformed nuclei in the TPDA NPs + laser group and GO NSs + laser group. Besides, the diminished Ki67-marked cells and elevated TUNEL-positive cells are observed in the TPDA NPs + laser group and GO NSs + laser group, revealing that TPDA NPs-mediated PTT significantly inhibits tumor progression and induces tumor cell apoptosis. Additionally, almost no abnormalities are monitored in the main organs including the heart, liver, spleen, lung, and kidney after different treatments, indicating no obvious adverse effects are induced by TPDA NPs-based PTT (Figure S39, Supporting


© 2024 Wiley-VCH GmbH

16163028, 0, Downloaded from https://onlinelibrary.wiley.com/doi/10.1002/adfm.202313528 by Tongji University, Wiley Online Library on [18/01/2024]. See the Terms and Conditions (https://onlinelibrary.wiley.com/terms-and-conditions) on Wiley Online Library for rules of use; OA articles are governed by the applicable Creative Commons License

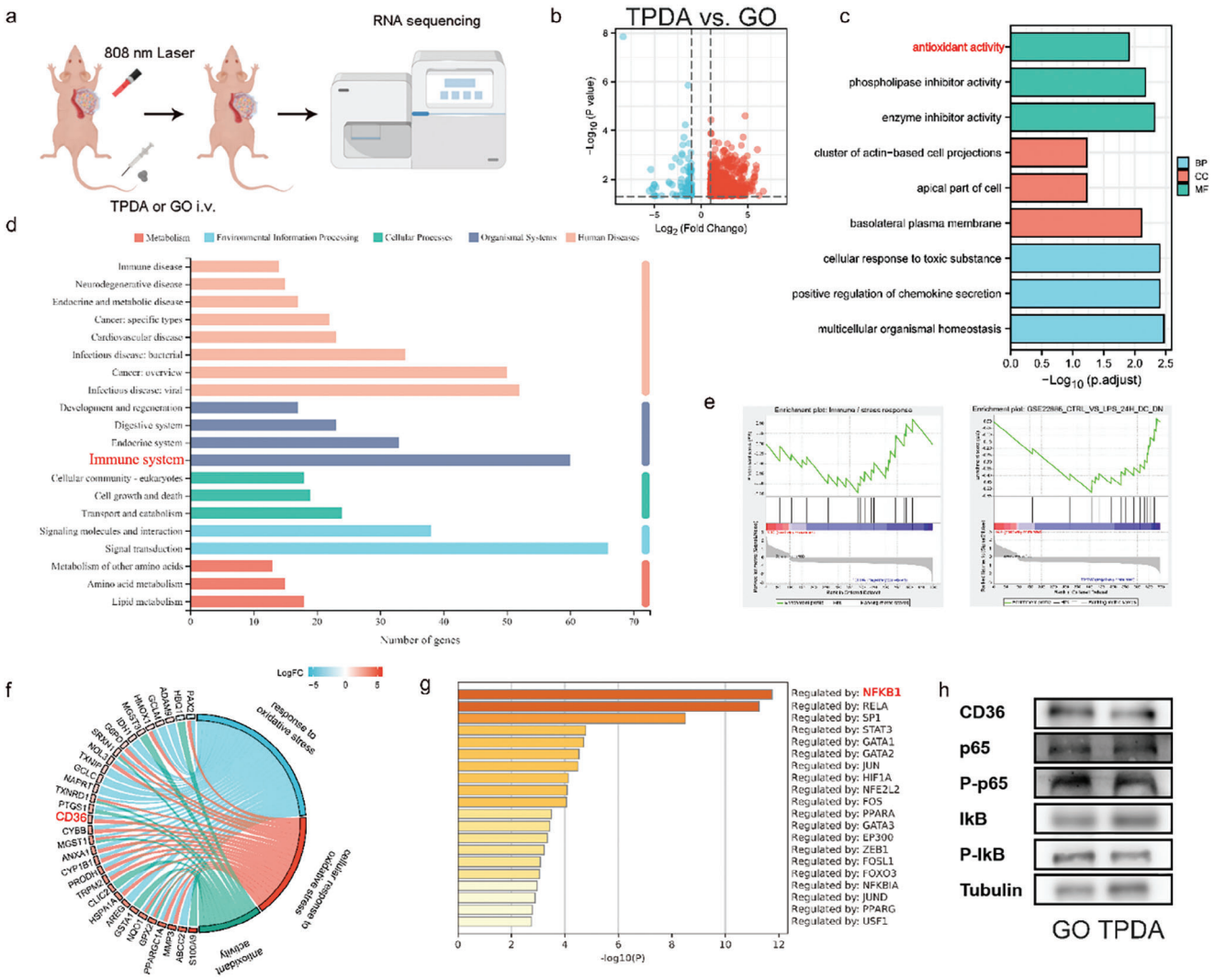


**Figure 9.** Inflammation-mediating mechanisms of TPDA NPs during PTT in vivo. a) Schematic illustration of RNA sequencing. b) Volcano plots exhibiting the up or down-regulation DEGs in this sequencing results. c) Gene Ontology analysis of the DEGs in the tumors with GO or TPDA treatments. d) KEGG annotation of the total DEGs. e) GSEA analyses of the DEGs in the tumors with different treatments. f) Enriched chord diagram of the Gene Ontology analyses. g) Analyzation of the TFs in the DEGs regulation. h) Western blot analysis of CD36, p65, p-p65, ikB, and p-ikB in tumors with different treatments.

Information). Subsequently, the PTT-related inflammation was investigated. Compared with GO NSs treatment, decreased expression of CD36 reveals the anti-inflammatory effect of TPDA NPs (Figure 8n; Figure S40, Supporting Information). Meanwhile, the 3-nitrotyrosine staining shows that TPDA NPs effectively alleviate PTT-induced inflammation (Figure 8n; Figure S40, Supporting Information). The decreased expression of IL-1$\beta$, IL-6, and TNF-$\alpha$, and the increased IL-10 expression further confirm the anti-inflammation activity of TPDA NPs during PTT (Figure 8n; Figure S40, Supporting Information).

The detailed therapeutic mechanisms behind regulating inflammation during the PTT process in PTT were further explored by RNA-sequencing (**Figure 9a**). 821 DEGs between the Gene Ontology and TPDA NPs groups are observed, accompanied by 668 DEGS upregulated and 153 downregulated (Figure 9b; Figure S41, Supporting Information). Subsequently, the Gene Ontology and KEGG analyses were conducted to assess the genetic changes between the two treatments (Figure 9c,d). The Gene Ontology molecular function of anti-oxidative activity was improved in the TPDA treatments compared to the GO group (Figure 9c). Meanwhile, the KEGG annotation analysis showed that the DEGs were enriched in the change of immune system in the TPDA PTT group (Figure 9d). GSEA results also indicated that the pathway changes involved in immune/stress and LPS response changed during the TPDA treatments compared to the GO treatments (Figure 9e). Moreover, the enriched chord diagram of DEGs, including the response to oxidative stress, cellular response to oxidative stress, and anti-oxidative activity, was further generated to concentrate on the vital functional DEGs in the TPDA treatment (Figure 9f). Consistent with the previous findings, CD36 was also considered the pivotal functional gene in the two groups. The TFs related to the DEGs were analyzed to assess the cellular gene changes after the TPDA treatment; the results indicated that the NF-$\kappa$B1 participated in the cellular


© 2024 Wiley-VCH GmbH

16163028, 0, Downloaded from https://onlinelibrary.wiley.com/doi/10.1002/adfm.202313528 by Tongji University, Wiley Online Library on [18/01/2024]. See the Terms and Conditions (https://onlinelibrary.wiley.com/terms-and-conditions) on Wiley Online Library for rules of use; OA articles are governed by the applicable Creative Commons License

protection (Figure 9g). Therefore, we estimated the changes in CD36 expression and NF-κB signaling pathway among the two groups (Figure 9h), which confirmed the hypothesis that TPDA NPs regulate the NF-κB signaling pathway by targeting CD36. Additionally, the DEGs between TPDA PTT and control groups were assessed to examine the anti-tumor performances (Figure S42, Supporting Information). We found that the increased DEGs induced by TPDA PTT were enriched in the cancer overview annotation of KEGG analysis (Figure S42a, Supporting Information). Simultaneously, the cAMP and MAPK signaling pathways, which participated in the tumor progression, were also changed after the TPDA PTT treatment (Figure S42b).[27] Together, our results demonstrate that TPDA NPs, as the antioxidant, exhibit a remarkable anti-tumor capability with no inflammatory injuries during PTT, thereby exhibiting promising prospects for clinical use.

## 3. Conclusion

In this study, we engineered biocompatible TPDA NPs, characterized by the SOD, CAT, POD, and GPx mimicking ability and enhanced photothermal efficiency. These NPs featured antioxidative and anti-tumor properties by effectively scavenging various RO/NSs and augmenting cell apoptosis during PTT, respectively. A series of systemic investigations revealed the excellent cellular protecting ability of TPDA NPs against oxidative stress in vitro, with the underlying mechanism of regulating the NF-κB signaling pathway by targeting CD36. In vivo experiments illustrated that TPDA NPs are an outstanding antioxidant against prostate inflammation, further protecting the sexual function damaged by EAP based on the alleviation of oxidative stress. Meanwhile, the enhanced photothermal conversion efficiency of TPDA NPs was tested for anti-tumor applications in prostate cancer. Furthermore, significant tumor cell death in vitro and tumor inhibition in vivo were observed after TPDA NPs treatment under subsequent 808 nm laser irradiation in the TPDA PTT. Importantly, the oxidative injuries caused by PTT were remarkably inhibited by the anti-inflammatory ability of TPDA, which was attributed to the molecular functions of CD36 and NF-κB signaling pathways. Together, our results suggest that the synthesized uniform TPDA NPs have robust RO/NSs-scavenging capability, improved photothermal efficiency, and excellent biocompatibility, and can function as anti-inflammatory and anti-tumor agents with a prominent therapeutic effect for the treatment of prostate diseases.

## Supporting Information

Supporting Information is available from the Wiley Online Library or from the author.

## Acknowledgements

K.W., W.M., and X.S. contributed equally to this work. This work was financially supported by National Key Research and Development Program of China (Grant No. 2021YFC2009300, 2021YFC2009305, and SQ2017YFSF090096), National Natural Science Foundation of China (Grant No. 52072393, 52272279, 81870517, 82270809, 81702507, and 32070646), Young Scientist Foundation of National Natural Science Foundation of China (Grant No. 82102085), Basic Research Program of Shanghai Municipal Government (Grant No. 21JC1406002), Shanghai Science and Technology Committee Rising-Star Program (Grant No. 21QA1403100), Shanghai Science and Technology Program (Grant No. 21142203400, 23JC1401203, 23JC1401200), Science and Technology Innovation Project in Health System of Shanghai Putuo District (Grant No. ptkwws202206), Wenzhou Basic Scientific Research Project (Grant No. Y20220138), Natural Science Foundation of Jiangsu Provience (Grant No. BK20230842), Program for Research-oriented Physician of Shanghai Tenth People's Hospital (Grant No. YNCR2A012, 2023YJXYSA016), and Climbing Talent Projects of Shanghai Tenth People's Hospital (Grant No. 2018SYPDRC046).

## Conflict of Interest

The authors declare no conflict of interest.

## Data Availability Statement

The data that support the findings of this study are available from the corresponding author upon reasonable request.

## Keywords

inflammation, nanomedicine, nanozyme, photothermal therapy, reactive oxygen/nitrogen species scavenging

Received: October 30, 2023
Published online:

[1] a) R. Zhang, S. Sutcliffe, E. Giovannucci, W. C. Willett, E. A. Platz, B. A. Rosner, J. D. Dimitrakoff, K. Wu, *J Urol* **2015**, *194*, 1295; b) S. Falahatkar, E. Shahab, K. Gholamjani Moghaddam, E. Kazemnezhad, *BJU Int.* **2015**, *116*, 641; c) D. S. Engeler, D. Hauri, H. John, *Eur Urol.* **2003**, *44*, 546.
[2] a) J. N. Krieger, *JAMA, J. Am. Med. Assoc.* **1999**, *282*, 236; b) G. Magistro, F. M. E. Wagenlehner, M. Grabe, W. Weidner, C. G. Stief, J. C. Nickel, *Eur Urol.* **2016**, *69*, 286.
[3] a) R. B. Alexander, S. Ponniah, J. Hasday, J. R. Hebel, *Urology* **1998**, *52*, 744; b) R. B. Nadler, A. E. Koch, E. A. Calhoun, P. L. Campbell, D. L. Pruden, C. L. Bennett, P. R. Yarnold, A. J. Schaeffer, *J Urol.* **2000**, *164*, 214; c) F. F. Pasqualotto, R. K. Sharma, J. M. Potts, D. R. Nelson, A. J. Thomas, A. Agarwal, *Urology* **2000**, *55*, 881; d) T. Kullisaar, S. Türk, M. Punab, R. Mändar, *Prostate* **2012**, *72*, 977.
[4] a) D. G. Tang, *Semin. Cancer Biol.* **2022**, *82*, 68; b) K. S. Sfanos, S. Yegnasubramanian, W. G. Nelson, A. M. De Marzo, *Nat. Rev. Urol.* **2018**, *15*, 11.
[5] H. Sung, J. Ferlay, R. L. Siegel, M. Laversanne, I. Soerjomataram, A. Jemal, F. Bray, *CA Cancer J Clin* **2021**, *71*, 209.
[6] M. S. Litwin, H.-J. Tan, *JAMA, J. Am. Med. Assoc.* **2017**, *317*, 2532.
[7] a) B. Yang, Y. Chen, J. Shi, *Chem. Rev.* **2019**, *119*, 4881; b) C. A. Ferreira, D. Ni, Z. T. Rosenkrans, W. Cai, *Nano Res.* **2018**, *11*, 4955; c) X. Bao, J. Zhao, J. Sun, M. Hu, X. Yang, *ACS Nano* **2018**, *12*, 8882; d) X. Dai, Y. Xie, W. Feng, Y. Chen, *Angew. Chem., Int. Ed.* **2023**, *n/a*, 202309160; e) M. Bao, K. Wang, J. Li, Y. Li, H. Zhu, M. Lu, Y. Zhang, Q. Fan, L. Han, K. Wang, D. Wang, Y. Gao, B. Peng, Z. Ming, W. Liu, *Acta Biomater.* **2023**, *161*, 250.
[8] a) M. E. Langston, M. Horn, S. Khan, R. Pakpahan, M. Doering, L. K. Dennis, S. Sutcliffe, *Cancer Epidemiol Biomarkers Prev.* **2019**, *28*, 1594;

 © 2024 Wiley-VCH GmbH

16163028, 0, Downloaded from https://onlinelibrary.wiley.com/doi/10.1002/adfm.202313528 by Tongji University, Wiley Online Library on [18/01/2024]. See the Terms and Conditions (https://onlinelibrary.wiley.com/terms-and-conditions) on Wiley Online Library for rules of use; OA articles are governed by the applicable Creative Commons License

b) S. Doat, M. Marous, X. Rebillard, B. Trétarre, P.-J. Lamy, P. Soares, O. Delbos, R. Thuret, B. Segui, S. Cénée, F. Menegaux, *Int. J. Cancer* **2018**, *143*, 1644; c) P. Verze, T. Cai, S. Lorenzetti, *Nat Rev Urol* **2016**, *13*, 379.

[9] a) A. I. S. B. Villaverde, J. Netherton, M. A. Baker, *Antioxidants* **2019**, *8*, 616; b) J. Song, X. Gao, Z. Tang, H. Li, Y. Ruan, Z. Liu, T. Wang, S. Wang, J. Liu, H. Jiang, *Andrology* **2020**; c) K. Nowicka-Bauer, B. Nixon, *Antioxidants* **2020**, *9*, 134; d) K. Wang, W. Mao, X. Song, M. Chen, W. Feng, B. Peng, Y. Chen, *Chem. Soc. Rev.* **2023**; e) P. Gharagozloo, R. J. Aitken, *Hum Reprod.* **2011**, *26*, 1628; f) T. Silberstein, I. Har-Vardi, A. Harlev, M. Friger, B. Hamou, T. Barac, E. Levitas, O. Saphier, *Oxid Med Cell Longev* **2016**, *2016*, 9140925; g) K. Tremellen, *Hum Reprod Update.* **2008**, *14*, 243.

[10] a) D. Bhowmick, S. Srivastava, P. D'silva, G. Mugesh, *Angew. Chem.* **2015**, *54*, 8449; b) Y. Zhang, Z. Wang, X. Li, L. Wang, M. Yin, L. Wang, N. Chen, C. Fan, H. Song, *Adv Mater.*, **2016**, *28*, 1387; c) W. Zhang, S. Hu, J.-J. Yin, W. He, W. Lu, M. Ma, N. Gu, Y. Zhang, *J. Am. Chem. Soc.* **2016**, *138*, 5860; d) Y. Huang, Z. Liu, C. Liu, E. Ju, Y. Zhang, J. Ren, X. Qu, *Angew. Chem., Int. Ed.* **2016**, *55*, 6646; e) K. Wang, Y. Zhang, W. Mao, W. Feng, S. Lu, J. Wan, X. Song, Y. Chen, B. Peng, *Adv. Funct. Mater.* **2021**.

[11] a) Y. Huang, Y. Fu, M. Li, D. Jiang, C. J. Kutyreff, J. W. Engle, X. Lan, W. Cai, T. Chen, *Angew. Chem. Int. Ed.*; b) M. Huo, L. Wang, Y. Wang, Y. Chen, J. Shi, *ACS Nano* **2019**, *13*, 2643; c) Y. Zhao, Z. Zhang, Z. Pan, Y. Liu, *Exploration* **2021**, *1*, 20210089.

[12] C. R. Dejulius, B. R. Dollinger, T. E. Kavanaugh, E. Dailing, F. Yu, S. Gulati, A. Miskalis, C. Zhang, J. Uddin, S. Dikalov, C. L. Duvall, *Bioconjug Chem.* **2021**, *32*, 928.

[13] F. Bernsmann, V. Ball, F. Addiego, A. Ponche, M. Michel, J. J. D. A. Gracio, V. Toniazzo, D. Ruch, *Langmuir* **2011**, *27*, 2819.

[14] a) C. P. Rubio, J. Hernández-Ruiz, S. Martinez-Subiela, A. Tvarijonaviciute, J. J. Ceron, *BMC Vet. Res.* **2016**, *12*, 166; b) R. Apak, M. Özyürek, K. GLü, E. Çapanoglu, *J. Agric. Food Chem.* **2016**, *64*, 997; c) I. Peluso, A. Cavaliere, M. Palmery, *J Biomed Sci* **2016**, *23*, 52.

[15] T. Liu, B. Xiao, F. Xiang, J. Tan, Z. Chen, X. Zhang, C. Wu, Z. Mao, G. Luo, X. Chen, J. Deng, *Nat. Commun.* **2020**, *11*, 2788.

[16] a) W. Zhang, S. Hu, J.-J. Yin, W. He, W. Lu, M. Ma, N. Gu, Y. Zhang, *J. Am. Chem. Soc.* **2016**, *138*, 5860; b) K. Y. Wang, Y. Zhang, W. P. Mao, W. Feng, S. T. Lu, J. Wan, X. R. Song, Y. Chen, B. Peng, *Adv. Funct. Mater.* **2022**, *32*, 2109221.

[17] Y. Guo, A. Baschieri, F. Mollica, L. Valgimigli, J. Cedrowski, G. Litwinienko, R. Amorati, *Angew. Chem., Int. Ed.* **2021**, *60*, 15220.

[18] R. T. Carroll, P. Galatsis, S. Borosky, K. K. Kopec, V. Kumar, J. S. Althaus, E. D. Hall, *Chem. Res. Toxicol.* **2000**, *13*, 294.

[19] a) L. Zhao, C. Zhang, X. Luo, P. Wang, W. Zhou, S. Zhong, Y. Xie, Y. Jiang, P. Yang, R. Tang, Q. Pan, A. R. Hall, T. V. Luong, J. Fan, Z. Varghese, J. F. Moorhead, M. Pinzani, Y. Chen, X. Z. Ruan, *J Hepatol* **2018**, *69*, 705; b) C. R. Stewart, L. M. Stuart, K. Wilkinson, J. M. Van Gils, J. Deng, A. Halle, K. J. Rayner, L. Boyer, R. Zhong, W. A. Frazier, A. Lacy-Hulbert, J. E. Khoury, D. T. Golenbock, K. J. Moore, *Nat. Immunol.* **2010**, *11*, 155; c) N. Sp, D. Y. Kang, D. H. Kim, J. H. Park, H. G. Lee, H. J. Kim, P. Darvin, Y. M. Park, Y. M. Yang, *Nutrients* **2018**, 10; d) M. Jiang, N. Wu, B. Xu, Y. Chu, X. Li, S. Su, D. Chen, W. Li, Y. Shi, X. Gao, H. Zhang, Z. Zhang, W. Du, Y. Nie, J. Liang, D. Fan, *Theranostics* **2019**, *9*, 5359.

[20] a) X. Song, G. Chen, C. Li, C. Yang, Y. Deng, *Inflammation* **2021**, *44*, 890; b) F. O. Dos Santos Gomes, A. C. Oliveira, E. L. Ribeiro, B. S. Da Silva, L. A. M. Dos Santos, I. T. De Lima, A. K. S. E. Silva, S. M. Da Rocha Araújo, T. Gonçalves, M. R. De Melo-Junior, C. A. Peixoto, *Inflamm Res* **2018**, *67*, 43.

[21] a) K. Wang, W. Mao, J. Ni, J. Xie, L. Yin, H. Zhang, T. Zhang, T. Xu, B. Peng, *Andrologia* **2021**, *53*, 14113; b) Y. Zhang, X. Li, K. Zhou, M. Zhou, K. Xia, Y. Xu, X. Sun, Y. Zhu, C. Cui, C. Deng, *Front Immunol* **2020**, *11*, 574212; c) K. Roman, C. Hall, A. J. Schaeffer, P. Thumbikat, *Prostate* **2020**, *80*, 28; d) Y. Liu, M. Tang, Q. Zhang, C. Li, R. Lv, H. Min, X. Zhou, *Inflammation* **2021**, *44*, 243; e) T. Huang, G. Wang, Y. Hu, H. Shi, K. Wang, L. Yin, B. Peng, *J Inflamm (Lond)* **2019**, *16*, 20.

[22] a) G. Magistro, F. M. E. Wagenlehner, M. Grabe, W. Weidner, C. G. Stief, J. C. Nickel, *Eur Urol* **2016**, *69*, 286; b) G. C. Wang, T. R. Huang, Y. Y. Hu, K. Y. Wang, H. Shi, L. Yin, B. Peng, *J Inflamm (Lond)* **2020**, *17*; c) D. Fan, W. Mao, G. Wang, H. Shi, Z. Wu, J. Xie, L. Yin, T. Xu, K. Wang, B. Peng, *Ann Palliat Med* **2021**, *10*, 1739.

[23] A. Mantovani, P. Allavena, A. Sica, F. Balkwill, *Nature* **2008**, *454*, 436.

[24] a) H. Huang, Y. Yang, X. Wang, F. Rehfeldt, K. Zhang, *Macromol. Rapid Commun.* **2019**, *40*, 1900263; b) X. Wang, L. Yang, P. Yang, W. Guo, Q.-P. Zhang, X. Liu, Y. Li, *Sci. China Chem.* **2020**, *63*, 1295; c) Y. Zou, X. Chen, P. Yang, G. Liang, Y. Yang, Z. Gu, Y. Li, *Sci. Adv.* **2020**, *6*, eabb4696.

[25] Y. Liu, K. Ai, J. Liu, M. Deng, Y. He, L. Lu, *Adv. Mater.* **2013**, *25*, 1353.

[26] M. Li, S. Li, H. Zhou, X. Tang, Y. Wu, W. Jiang, Z. Tian, X. Zhou, X. Yang, Y. Wang, *Nat. Commun.* **2020**, *11*, 1126.

[27] a) K. Jiang, G. Yao, L. Hu, Y. Yan, J. Liu, J. Shi, Y. Chang, Y. Zhang, D. Liang, D. Shen, G. Zhang, S. Meng, H. Piao, *Cell Death Dis.* **2020**, *11*, 230; b) J. Y. Fang, B. C. Richardson, *Lancet Oncol.* **2005**, *6*, 322.



© 2024 Wiley-VCH GmbH

16163028, 0, Downloaded from https://onlinelibrary.wiley.com/doi/10.1002/adfm.202313528 by Tongji University, Wiley Online Library on [18/01/2024]. See the Terms and Conditions (https://onlinelibrary.wiley.com/terms-and-conditions) on Wiley Online Library for rules of use; OA articles are governed by the applicable Creative Commons License